Gradient Monte Carlo simulations: Hard spheres in spatially varying temperature and gravitational fields

Anuja Seth Mehrotra and Sanjay Puri
School of Physical Sciences, Jawaharlal Nehru University, New Delhi, 110067, India

D. V. Khakhar*
Department of Chemical Engineering, Indian Institute of Technology Bombay, Powai, Mumbai, 400076, India
(Received 20 March 2010; revised manuscript received 18 March 2011; published 30 June 2011)

There are many physical situations where particles experience external fields or are in a nonisothermal environment. Monte Carlo (MC) simulations can be useful to understand such experimental systems at steady state. Within this context, we formulate a general framework to study these systems via inhomogeneous MC simulations incorporating spatially varying temperature and gravitational fields. Using this approach we study granular materials consisting of hard spheres in an external field with either uniform or nonuniform temperature. We present comprehensive results from our MC simulations and compare these with theoretical results based on the Carnahan-Starling equation of state.

DOI: 10.1103/PhysRevE.83.061306 PACS number(s): 45.70.−n, 05.10.Ln

I. INTRODUCTION

Monte Carlo (MC) simulations are now a standard tool to study the equilibrium properties of molecular systems [1,2]. The MC approach involves a numerical integration over phase space, sampling configurations depending on their probability of occurrence. The method is attractive because of its simplicity and lower computational requirements relative to molecular dynamics (MD) simulations [3]. Over the five decades since it was first proposed [4,5], many refinements and variations have been incorporated in the MC method. For example, an important extension is the direct simulation Monte Carlo method, which is a combination of MC and MD approaches [6].

There are many physical situations in which field gradients exist naturally in a system. For example, a gas in a gravitational field exhibits a spatial variation in number density. On the other hand, an imposed temperature gradient in the system will also result in variation of the number density. Such systems are not in thermodynamic equilibrium, and the steady state (time-invariant state) results from a balance of fluxes. The standard approach for analysis of these systems is to use transport equations with the assumption of local thermodynamic equilibrium. Thus the hydrostatic balance equation in conjunction with an equation of state may be used to analyze a gas in a gravitational field (ref. Sec. II A). In this paper we use MC simulations to study steady-state systems with gradients as defined above. Apart from the relevance to statistical physics, such systems are of great importance in the study of granular materials [7–10], as we discuss below.

There have been a number of MC studies of inhomogeneous systems, e.g., colloids [11–21], biophysics of receptor cells [22], inhomogeneous percolation [23], etc. In general, the MC approach has proved very useful to study both static and dynamic properties of powders [24–27]. As shown in several studies [28,29], the equation of state for slightly inelastic particles is the same as that for elastic particles. Thus the thermodynamic properties of granular materials can be obtained by MC for slightly inelastic grains. Isothermal MC simulations were used by Khakhar *et al.* [30,31] to study hard sphere mixtures in a gravitational field, in the context of granular segregation. At low densities there was good agreement between simulation results and the predictions of a continuum theory. Seibert and Burns [32] proposed an MC method for analyzing fluidized beds and compared their simulations to experimental results. Although the MC method has been widely used to study inhomogeneous systems, there has not been a detailed analysis of its accuracy for calculation of equilibrium thermodynamic properties in the presence of spatial inhomogeneity. MC simulations have not been applied to systems with a spatially varying temperature field.

In this paper we propose and test a general method for Monte Carlo simulation of systems with a spatially varying temperature field. We also examine the accuracy of MC simulations for obtaining thermodynamic properties in systems with significant gradients. Such inhomogeneous MC simulations are particularly relevant for granular chute flows [10,33]. In these flows, the solids' volume fraction is nearly uniform but the temperature varies with height [33]. The imposition of gradients is also useful for obtaining thermodynamic properties spanning a range of states in a single simulation. Here a simple model system, for which theoretical results are available, is used. MC simulations of the system incorporating gradients in the gravitational field and the temperature are carried out and the computed results are compared to an established equation of state.

This paper is organized as follows. In Sec. II we present the theoretical background for studying inhomogeneous systems. In Sec. III we present details of our numerical simulations. The numerical results are presented in Sec. IV. Finally, we end this paper with a summary and discussion in Sec. V.

*khakhar@iitb.ac.in

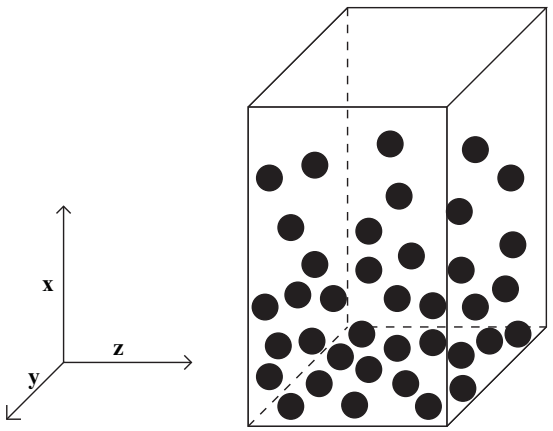

FIG. 1. Schematic view of a granular material consisting of hard spheres in a gravitational field (acting along the x direction). We impose periodic boundary conditions in the y,z directions, and reflecting boundary conditions in the x direction. The upper x boundary is taken to be high enough so that the density becomes negligible there.

II. THEORETICAL BACKGROUND

We consider elastic hard spheres in a gravitational field as shown in Fig. 1. The system is analogous to the classical problem of Brownian particles in a gravitational field studied by Perrin [34]. The particles are identical and have a diameter d and mass m. The base is an elastic planar surface. The system is thus nondissipative. We would like to mimic the equilibrium number density profiles obtained in dissipative systems (e.g., granular flows) by considering (i) a spatially varying gravitational field of the form

$$a(x) = g\exp(\alpha x), \tag{1}$$

where a is the acceleration experienced by a particle at height x, and (ii) an imposed temperature profile of the form

$$T(x) = T_0\exp(-\beta x). \tag{2}$$

In Eqs. (1) and (2), g is the acceleration due to gravity, T_0 is the temperature at the base, and α,β are constants. Since we are interested in granular systems, the temperature used is the granular temperature $T = m\langle v^2\rangle/2$ [35], where $\langle v^2\rangle$ is the mean-square fluctuation velocity of the grains. Thus T is the kinetic energy (per particle) associated with the fluctuation velocity. The results presented below are also applicable to molecular systems but with T replaced by k_BT, where k_B is the Boltzmann constant and T is the usual thermodynamic temperature.

A. Number Density Profile

The steady-state number density profile is obtained as follows for the above system. The stress balance equation is

$$\frac{dP}{dx} = -mna, \tag{3}$$

where P is the pressure, ma is the net downward force, and n is the number density of the particles. Further, assuming local equilibrium, we have from the equation of state

$$P = nTZ(\nu), \tag{4}$$

where $Z(\nu)$ is the compressibility factor and $\nu = n\pi d^3/6$ is the volume fraction of the particles. Here we use the Carnahan-Starling (CS) equation of state [36], for which the compressibility factor is given by

$$Z(\nu) = \frac{1+\nu+\nu^2-\nu^3}{(1-\nu)^3}. \tag{5}$$

Combining Eqs. (3) and (4), we obtain

$$\frac{d(nTZ)}{dx} = -mna, \tag{6}$$

which upon rearrangement yields

$$\frac{d\ln n}{dx} = -\frac{(ma)/(TZ) + d\ln T/dx}{1 + d\ln Z/d\ln\nu}. \tag{7}$$

Equation (7) can be solved to obtain the static profile $n(x)$ for a specified gravitational field $a(x)$ and temperature profile $T(x)$.

For the assumed profiles specified in Eqs. (1) and (2), Eq. (7) becomes

$$\frac{d\ln n}{dx} = -\frac{(mg)/(T_0Z)e^{(\alpha+\beta)x} - \beta}{1 + d\ln Z/d\ln\nu}. \tag{8}$$

A numerical solution is necessary for the general case. However, it is relevant to understand the ideal gas limit, which serves as a reference point. In the limit of low volume fractions ($\nu \ll 1$), ideal gas behavior is obtained ($Z = 1$) and Eq. (8) reduces to

$$\frac{d\ln n}{dx} = -\frac{mg}{T_0}e^{(\alpha+\beta)x} + \beta. \tag{9}$$

Equation (9) has the solution

$$\ln\left(\frac{n}{n_0}\right) = -\frac{mg}{(\alpha+\beta)T_0}[e^{(\alpha+\beta)x} - 1] + \beta x, \tag{10}$$

where n_0 is the number density at the base ($x = 0$). For the case of a constant field ($\alpha = 0$) and a uniform temperature ($\beta = 0$), the preceding equation reduces to

$$n(x) = n_0\exp\left(-\frac{mgx}{T_0}\right), \tag{11}$$

which is a well-known result [34].

B. Importance Sampling

We consider next the theoretical basis of MC simulations for the system defined above. We begin with the case of a constant gravitational field and a uniform temperature, and then generalize to allow for a spatially varying $a(x)$ and $T(x)$. In an MC simulation, we start off with an initial configuration and subject the system to a series of sequential random perturbations. Each proposed change is accepted with a certain probability which satisfies the detailed-balance condition [1,2] so as to drive the system to equilibrium. According to the Metropolis algorithm [1,2], the probability of acceptance of a step is given by

$$p = \begin{cases} \exp(-\Delta E/T_0), & \Delta E > 0, \\ 1, & \Delta E < 0, \end{cases} \tag{12}$$

where ΔE is the change in energy due to the perturbation, and T_0 is the uniform temperature. Thus all changes which

result in a decrease of energy are accepted, but only a fraction p of perturbations which result in an increase of energy are accepted. Let us next obtain expressions for the acceptance probability for the different cases considered here. We assume that the velocity distribution is equilibrated and focus on configurational changes arising from changes of particle positions.

In the case of a uniform gravitational field ($a = g$), the change in energy due to the displacement of a single particle by Δx is

$$\Delta E = mg\Delta x, \tag{13}$$

if the displacement results in no overlap of particles; and $\Delta E = \infty$, if there is an overlap. For a uniform temperature ($T = T_0$), the probability of acceptance of this displacement is

$$p = \exp\left(-\frac{mg\Delta x}{T_0}\right). \tag{14}$$

Here, and subsequently, we write down only the expression for $\Delta E > 0$ – for $\Delta E < 0$, $p = 1$ always. Clearly, all displacements which result in overlaps are rejected ($p = 0$). Equation (14) indicates that all downward steps are accepted, and upward steps are accepted with a probability $p(\Delta x)$.

Next, consider a spatially varying gravitational field $a(x)$ and a uniform temperature ($T = T_0$). In this case, the change in energy due to the displacement of a single particle which causes no particle overlap is

$$\Delta E = \int_{x_0}^{x_0+\Delta x} ma\ dx, \tag{15}$$

where x_0 is the initial height of the particle. For the gravitational field in Eq. (1),

$$p = \exp\left[-\frac{mge^{\alpha x_0}}{\alpha T_0}(e^{\alpha\Delta x} - 1)\right]. \tag{16}$$

This reduces to Eq. (14) in the limit $\alpha \to 0$, as required.

Finally, we consider the case of a uniform gravitational field ($a = g$) but a spatially varying temperature:

$$T = T_0 f(x). \tag{17}$$

The Metropolis algorithm is not valid in this case, and our simulations show that a direct substitution of Eq. (17) into Eq. (12) gives incorrect results. Here we obtain an expression for the acceptance probability by constructing an equivalent isothermal system but with a varying gravitational field, which gives an identical number density profile. By substituting Eq. (17) in Eq. (6) with $a = g$, we obtain

$$\frac{d(nT_0Z)}{dx} = -\frac{mgn}{f} - \frac{nT_0Z}{f}\frac{df}{dx}. \tag{18}$$

Equation (18) may be rewritten as

$$\frac{d(nT_0Z)}{dx} = -mng_e, \tag{19}$$

where

$$g_e = \frac{g}{f} + \frac{T_0Z}{mf}\frac{df}{dx}. \tag{20}$$

Equation (19) shows that the nonisothermal system is equivalent to an isothermal system at temperature T_0 but with an effective (spatially varying) gravitational field $g_e(x)$. The change in potential energy due to displacement of a single particle with no overlap, in the equivalent isothermal system, is given by

$$\Delta E = \int_{x_0}^{x_0+\Delta x} mg_e dx. \tag{21}$$

The corresponding acceptance probability for the step is

$$p = \exp\left(-\frac{\Delta E}{T_0}\right). \tag{22}$$

Next we obtain $g_e(x)$ as a functional of $n(x)$. From Eq. (3) we obtain the pressure profile as

$$P(x) = mg\int_x^\infty n(x')dx', \tag{23}$$

where the pressure far from the base is taken to be zero, $P(\infty) = 0$. By using $Z = P/(nT)$ in Eq. (20), we obtain the effective gravitational field:

$$g_e = \frac{g}{f} + \frac{g}{nf^2}\frac{df}{dx}\int_x^\infty n(x')dx'. \tag{24}$$

Thus given $n(x)$, $g_e(x)$ can be computed for any $f(x)$. Combining Eqs. (24) and (21), we obtain

$$p = \exp\left[-\frac{mg}{T_0}\int_{x_0}^{x_0+\Delta x}\left(\frac{1}{f} + \frac{1}{nf^2}\frac{df}{dx}\int_x^\infty n(x')dx'\right)dx\right]. \tag{25}$$

Finally, by substituting $f(x) = e^{-\beta x}$ from Eq. (2), we obtain

$$p = \exp\left[-\frac{mge^{\beta x_0}}{\beta T_0}(e^{\beta\Delta x} - 1) + \frac{mg\beta}{T_0}\int_{x_0}^{x_0+\Delta x}\frac{e^{\beta x}}{n} \times \left(\int_x^\infty n(x')dx'\right)dx\right]. \tag{26}$$

The first term in the exponential is similar to that in Eq. (16). However, the second term depends on the local number density and must be determined numerically.

It is straightforward to obtain the MC transition probability for the case where both the gravitational field and temperature are spatially varying functions. For the sake of brevity, we do not present the resulting expressions here.

C. Dimensionless Equations

We next rescale variables to put the above equations in dimensionless form: $\bar{x} = x/d, \bar{\alpha} = \alpha d, \bar{\beta} = \beta d, \bar{T} = T/(mgd)$, $\bar{n} = nd^3, \bar{P} = Pd^2/(mg), \bar{a} = a/g$, where the overbars denote dimensionless quantities. The governing equation for the number density profile in dimensionless form is then

$$\frac{d\ln\bar{n}}{d\bar{x}} = -\frac{(1)/(\bar{T}_0Z)e^{(\bar{\alpha}+\bar{\beta})\bar{x}} - \bar{\beta}}{1 + d\ln Z/d\ln\nu}, \tag{27}$$

and the number density profile for an ideal gas is

$$\ln\left(\frac{\bar{n}}{\bar{n}_0}\right) = -\frac{1}{(\bar{\alpha}+\bar{\beta})\bar{T}_0}[e^{(\bar{\alpha}+\bar{\beta})\bar{x}} - 1] + \bar{\beta}\bar{x}. \tag{28}$$

The acceptance probability for an isothermal system with a uniform gravitational field is

$$p = \exp\left(-\frac{\Delta\bar{x}}{\bar{T}_0}\right). \tag{29}$$

This system is characterized by one parameter $\bar{T}_0$. The corresponding expression for an isothermal system with a spatially varying field is

$$p = \exp\left[-\frac{e^{\bar{\alpha}\bar{x}_0}}{\bar{\alpha}\bar{T}_0}(e^{\bar{\alpha}\Delta\bar{x}} - 1)\right]. \tag{30}$$

This system is characterized by two parameters $\bar{T}_0, \bar{\alpha}$. Finally, the acceptance probability for a system with a spatially varying temperature and a uniform gravitational field is

$$p = \exp\left[-\frac{e^{\bar{\beta}\bar{x}_0}}{\bar{\beta}\bar{T}_0}(e^{\bar{\beta}\Delta\bar{x}} - 1) - \frac{1}{\bar{\beta}\bar{T}_0} \times \int_{\bar{x}_0}^{\bar{x}_0+\Delta\bar{x}} \left(\frac{e^{\bar{\beta}\bar{x}}}{\bar{n}} \int_{\bar{x}}^{\infty} \bar{n}(\bar{x}')dx'\right) dx\right]. \tag{31}$$

Again, this system is characterized by two parameters $\bar{T}_0, \bar{\beta}$. In our subsequent discussion, we drop the bars and always work with dimensionless variables.

III. COMPUTATIONAL DETAILS

The simulation space consists of reflecting boundaries in the x direction (both top and bottom) and periodic boundaries in the y and z directions. Simulations are performed by initially placing 25,000 particles randomly in the box, which extends $400 \times 25 \times 25$ particle diameters in the x, y, and z directions, respectively. Particles are inserted sequentially, with the coordinates of each particle being assigned using a random number generator. If a new particle does not overlap with any existing particle, then its position is accepted. Thus the initial configuration consists of particles uniformly distributed in the box with average number density $n_{\rm av} = 0.1$.

The above configuration is the starting point of our MC simulations. Each particle is given a uniform random displacement $(\Delta x, \Delta y, \Delta z)$ in the range $(-S, S)$. If the displacement does not result in the overlap of particles, it is accepted with the probability $p(\Delta x)$ given in Sec. II C. A Monte Carlo step (MCS) denotes a complete cycle of trial displacements of all particles. Standard procedures (binning, linked lists, etc.) [3] are used for enhancing computational efficiency while checking for particle overlap.

The number density profile $n(x)$ is calculated for each MCS using horizontal bins of height 0.1 particle diameter. Here $n(x)$ denotes the number density in a bin at position x. Recall that $n(x)$ is required for computing the acceptance probability for the system with a spatially varying temperature [cf. Eq. (31)]. The maximum displacement used in the computations is $S = 0.75$ in all cases except $\alpha = 0.1$, for which $S = 0.25$ is used.

The system is assumed to have reached steady state when the center of mass becomes approximately constant in time. As shown in the following section, a steady state is reached well within 5×10^5 MCSs in all cases. Thus the first 5×10^5 MCSs are discarded and data are collected for five subsequent intervals of 10^5 MCSs each. The results reported are an average over the five intervals (i.e., 5×10^5 MCSs) and the average absolute deviation of the five runs is calculated as a measure of the computational error. The steady-state number density profile $[n(x)]$ is the primary measurement. The pressure profile $P(x)$ is computed from the number density profile using Eq. (3), and the results are compared to the predictions of the CS equation of state. We note that the calculation of the pressure in systems with an applied field (i.e., inhomogeneous MC) is very simple, compared to homogeneous MC. A similar approach based on experimental measurements of number density profiles for sedimenting colloidal particles has been used by Piazza *et al.* [37].

IV. NUMERICAL RESULTS

We present below results for the three different systems discussed above: (a) uniform temperature and uniform external field; (b) uniform temperature and spatially varying external field; and (c) spatially varying temperature and uniform external field.

A. Isothermal System in a Uniform Gravitational Field

Let us first consider an isothermal system in a uniform gravitational field $a = 1$ (in dimensionless units). Figure 2 shows the variation of the center of mass (h_c) with MCS. The initial condition consisted of a homogeneous distribution of particles. Gravity tends to settle the particles, resulting in decrease of h_c with MCS. The particles have kinetic energy (characterized by the granular temperature) which restricts complete settling. As the MC simulation proceeds, the system reaches a steady-state configuration where h_c does not change further, as shown in Fig. 2. As can be seen from the inset in Fig. 2, the saturation value of h_c (h_c^s) increases linearly with T_0 at high temperatures. This is because a significant volume in these systems has a low particle number density, approaching the ideal gas limit, in which volume is proportional to temperature at a constant pressure.

Figure 3(a) shows the variation of the steady-state number density (n) with height (x) for different values of T_0. The highest number density occurs at the base, where the pressure

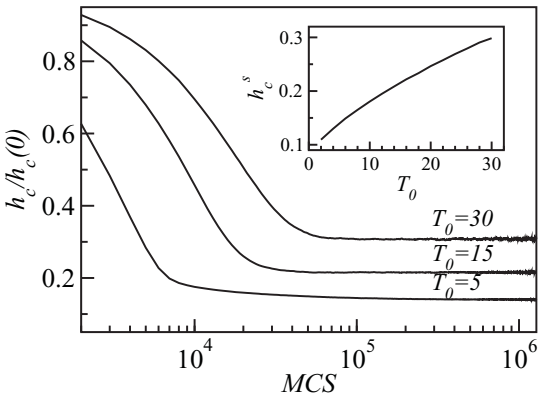

FIG. 2. Variation of the height of the center of mass (h_c) with MCS (t). The results correspond to an isothermal constant-gravity system with $T_0 = 5, 15, 30$. Inset: Plot of the saturation value of h_c versus temperature.

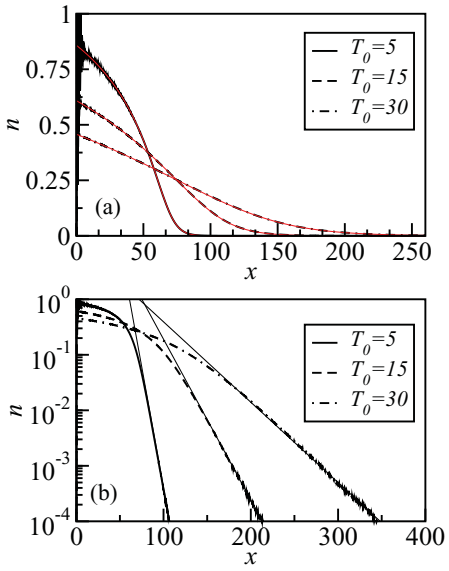

FIG. 3. (Color online) (a) Variation of the number density (n) with height (x) at steady state for an isothermal constant-gravity system for different values of T_0 as indicated. The solid lines are predictions of Eq. (27). (b) Linear-log plot of data sets in (a). The solid lines denote the corresponding ideal gas profiles from Eq. (28).

is the highest. The bed expands with increasing T_0, and the gradients in number density reduce. In all cases, the density decays to a very small value ($< 10^{-4}$) at the top of the box ($x = 400$), validating the assumption $P(\infty) = 0$, which is required to calculate the pressure profile. Figure 3(b) is a linear-log plot of the data in Fig. 3(a). The solid lines denote the ideal gas behavior in Eq. (28) — this is the appropriate limit at low densities and pressures. The solid lines in Fig. 3(a) are the predictions of Eq. (27) obtained by numerical integration. There is good agreement between theory and simulations.

We study next the variation of $n(x)$ close to the base ($x = 0$). Figure 4 shows $n(x)$ vs x for the data in Fig. 3(a). The density profile shows a layered structure due to the discreteness of the particles, in conjunction with an exponentially decaying envelope. At the lowest temperature ($T_0 = 5$), five layers are clearly evident, and the number of layers decreases with increase in T_0. A quantitative measure of the morphology is

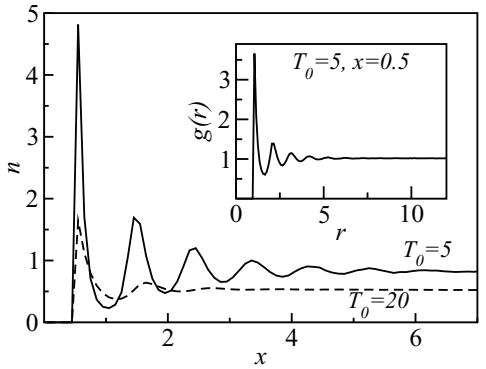

FIG. 4. Analogous to Fig. 3(a), but $n(x)$ is shown in a region close to the base. Inset: Radial distribution function [$g(r)$] of particles in the lateral (yz) plane for $x = 0.5$ and $T_0 = 5$.

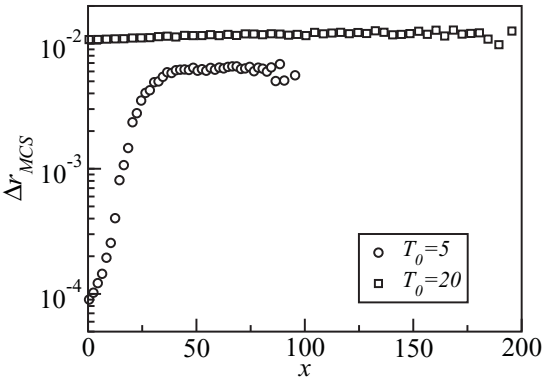

FIG. 5. Variation of the mean displacement per Monte Carlo step (Δr_{MCS}) with height (x) for the temperatures indicated in the legend.

the radial distribution function $g(r)$ in the lateral direction, where $r = (y^2 + z^2)^{1/2}$. The inset in Fig. 4 shows $g(r)$ vs r, computed for the particles in the horizontal bin corresponding to the lowermost peak position ($x = 0.5$) for $T_0 = 5$ in Fig. 4. The radial distribution function resembles that for a liquid and indicates the existence of a disordered state near the base.

Figure 5 shows the variation of the mean displacement per MCS (Δr_{MCS}) with height for the two cases shown in Fig. 3. Δr_{MCS} is an average over only accepted displacements in a bin and is hence a measure of the local mobility of particles. At $T_0 = 20$, the relatively large values of Δr_{MCS} indicate that the system is in a fluidlike state and the layering seen is a boundary effect of the flat base ($x = 0$). At $T_0 = 5$, however, the sharp decrease in Δr_{MCS} close to the base indicates the approach to a glassy state. In the comparisons made below, we omit the layered region near the base (five to eight particle diameters) in which boundary effects are significant.

Figure 6 shows a comparison of the pressure (P)-solids' volume fraction (ν) profiles from our MC simulations with the CS equation of state. There is very good agreement between them. In spite of significant gradients in number density, the inhomogeneous MC method yields the local equilibrium pressure. This is true even for $T_0 = 5$, where a sharp decrease

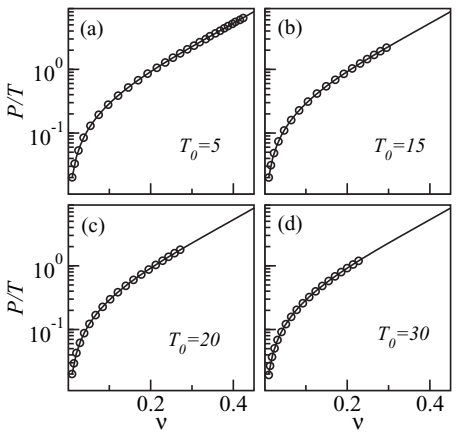

FIG. 6. Variation of the normalized pressure (P/T_0) with volume fraction (ν) for isothermal constant-gravity systems. We show MC results for $T_0 = 5,15,30$. The solid line denotes the CS equation of state.

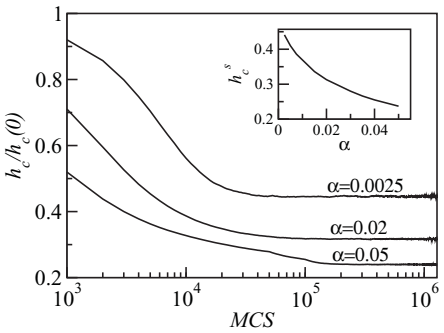

FIG. 7. Variation of h_c with t for an isothermal ($T_0 = 20$) system with a spatially varying gravitational field $a(x) = \exp(\alpha x)$. We show results for $\alpha = 0.0025, 0.02, 0.05$. Inset: Plot of the saturation value of h_c versus the field gradient parameter, α.

in Δr_{MCS} is seen near the base. Thus the system remains fluidlike and follows the equilibrium CS equation everywhere except in the boundary region (eight particle diameters for $T_0 = 5$). Furthermore, a single simulation is able to generate a pressure vs volume fraction equilibrium graph over a wide range of volume fractions, which would normally require a large number of homogeneous simulations.

B. Isothermal System in a Spatially Varying Gravitational Field

Figure 7 shows the variation of h_c with MCS for an isothermal system with $T_0 = 20$, and a spatially varying gravitational field, $a(x) = \exp(\alpha x)$. The initial distribution of particles is homogeneous. As before, the gravitational field settles the particles, resulting in a reduction of h_c with increasing MCS. The system reaches a steady-state configuration, characterized by h_c becoming approximately constant. The saturation value h_c^s decreases with increasing field gradient α, as shown in the inset of Fig. 7. This implies that the equilibrium configurations are more compact at higher field gradients.

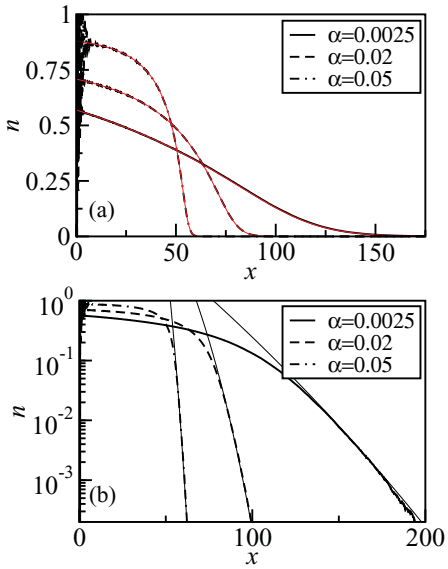

FIG. 8. (Color online) (a) Variation of n with x at steady state for an isothermal ($T_0 = 20$) system with a spatially varying field. We show results for $\alpha = 0.0025, 0.02, 0.05$. (b) Linear-log plot of data sets in (a). The solid lines denote the corresponding ideal gas profiles from the dimensionless form of Eq. (28).

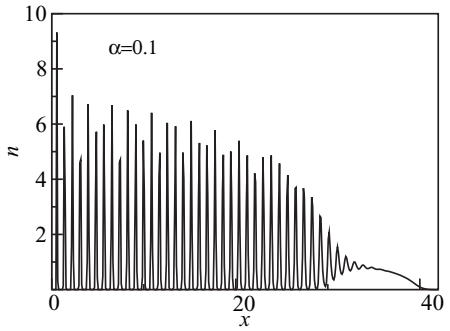

FIG. 9. (a) Variation of n with x at steady state for an isothermal ($T_0 = 20$) system with a spatially varying field for $\alpha = 0.1$.

Figure 8(a) shows $n(x)$ vs x for $T_0 = 20$ and different values of α. The highest number density occurs at the base where the pressure is the highest. The bed becomes more densely packed with increasing α and the density gradients reduce in the bulk but increase near the free surface. This "squeezing" of the bed is because the weight of a particle increases with height as a result of the field gradient. The total pressure at the base of the bed also increases with α, and consequently, there is an increase in the number density at the base with increasing α (Fig. 8(a)). The solid lines in the figure are predictions of Eq. (27) and show very good agreement with the MC results. Figure 8(b) is a linear-log plot of the data sets in Fig. 8(a). For small values of n, the behavior is consistent with the ideal gas profile in Eq. (28).

In Fig. 9 we plot $n(x)$ vs x for a relatively higher value of the field gradient parameter, $\alpha = 0.1$. A significant fraction of the system is in a layered state with an average layer spacing of $\Delta x = 0.86$, considering the bottom 20 layers. This is close to the hcp structure value of $\Delta x = 0.82$. The positions of the particles, shown in Fig. 10, indicate an ordered structure with

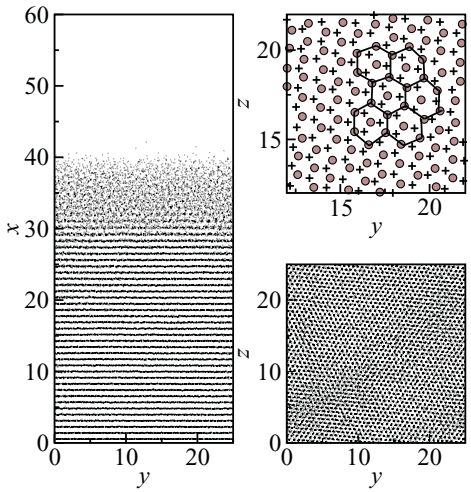

FIG. 10. (Color online) Left, bottom right: Positions of all particles for an isothermal ($T_0 = 20$) system with a spatially varying field for $\alpha = 0.1$. Top right: magnified view of the horizontal layers at $x = 0.5$ (circle) and at $x = 1.3$ (plus) showing a staggered hexagonal packing in adjacent layers, characteristic of hcp.

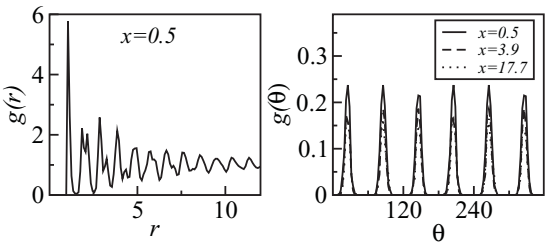

FIG. 11. Distribution functions for an isothermal ($T_0 = 20$) system with a spatially varying field for $\alpha = 0.1$. Left: Radial distribution function $g(r)$ computed in the horizontal bin at $x = 0.5$. Right: Angular distribution function $g(\theta)$ for nearest neighbors ($r < 1.2$) computed in horizontal bins at different x as indicated.

the magnified view indicating hexagonal packing of layers, with adjacent layers stacked in a staggered arrangement that is characteristic of an hcp structure. The radial distribution function [$g(r)$] at the base (Fig. 11) also indicates an ordered structure, while the angular distribution function [$g(\theta)$] for the nearest neighbors ($r < 1.2$) implies a hexagonal packing in the layer, since the peaks are separated by an angle of 60 deg.

The variation of mean displacement with height in the system is shown in Fig. 12 for the different field gradients parameterized by α. The data indicate that the system is fluidlike throughout for $\alpha = 0.0025$. There is a reduction in mobility near the base for $\alpha = 0.05$, implying a tendency toward glass formation. The sharp decrease in mobility at $x \approx 26$ for $\alpha = 0.1$ is typical of a phase change and indicates freezing near the base for $\alpha = 0.1$, in concurrence with the above results.

Figure 13 shows a comparison of the MC results of pressure (P) vs volume fraction (ν) to the predictions of the CS equation, excluding the data from the frozen and boundary regions. There is very good agreement between the MC results and the CS equation for all the values of α considered. We note that the gradients are much larger in this case as compared to the constant field case (Fig. 3), yet the accuracy of the MC computation remains high.

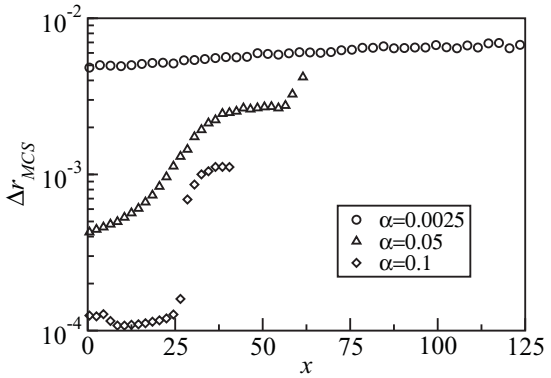

FIG. 12. Variation of the mean displacement per Monte Carlo step (Δr_{MCS}) with height (x) for the different values of the field gradient parameter (α) indicated in the legend.

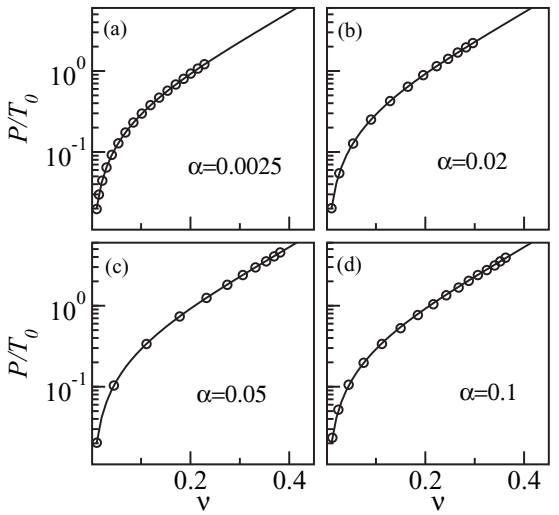

FIG. 13. Variation of P/T_0 with ν for an isothermal system ($T_0 = 20$) with a spatially varying field for the different values of the field gradient parameter (α) indicated. The solid line denotes the predictions of the CS equation of state.

C. Nonisothermal System in a Uniform Gravitational Field

Finally, we study a system with a spatially varying temperature [$T = T_0 \exp(-\beta x)$ with $T_0 = 20$] and a uniform gravitational field ($a = 1$). Figure 14(a) shows $n(x)$ vs x for different values of the temperature gradient β. The corresponding linear-log plot is shown in Fig. 14(b). In this case, the density decays monotonically with x only for small values of β. For larger values of β [see Fig. 14(a)], the density maximum is determined by the competition between the gravitational field and the decreasing temperature (with

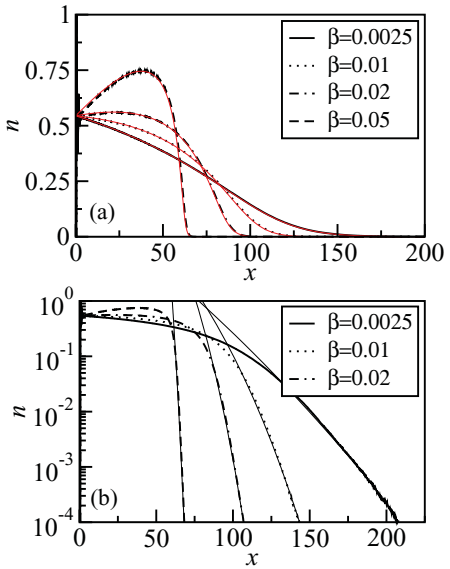

FIG. 14. (Color online) (a) Variation of n with x at steady state for a constant-gravity system with a spatially varying temperature $T(x) = T_0 \exp(-\beta x)$ with $T_0 = 20$ for different values of β. The solid lines are predictions of Eq. (27). (b) Linear-log plot of data sets in (a). The solid lines denote the corresponding ideal gas profiles from the dimensionless form of Eq. (28).

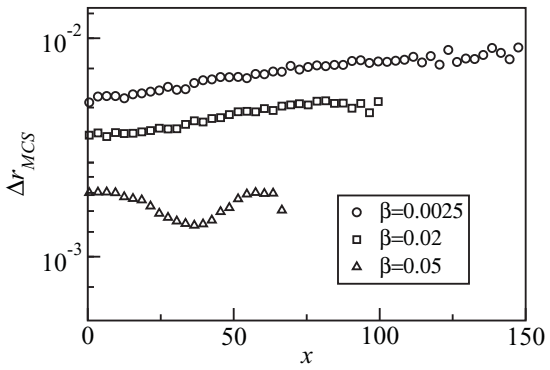

FIG. 15. Variation of the mean displacement per Monte Carlo step (Δr_{MCS}) with height (x) for the different values of the temperature gradient parameter (β) indicated in the legend.

height). The maximum is located at $x_m = \beta^{-1}\ln(T_0 Z\beta)$ in dimensionless units [cf. Eq. (27), with $\alpha = 0$]. As in the previous cases, predictions of Eq. (27) [Fig. 14(a)] and Eq. (28) [Fig. 14(b), low-number-density region] closely match the MC results.

Figure 15 shows the mean motion per Monte Carlo step (Δr_{MCS}) for the different values of β studied. The system is in a fluidlike state for all cases, in spite of the significant number fraction gradients. Further, no significant layering is seen even at the highest value of β. Both these results are a consequence of the highest temperatures being at the base ($x = 0$).

We plot $P/T(x)$ vs ν in Fig. 16 for different values of β, excluding the data in the boundary region. Again, the MC data is in excellent agreement with the CS equation over an extended range of temperature values [$T \in (0^+,20)$]. This validates the gradient MC method for nonisothermal systems.

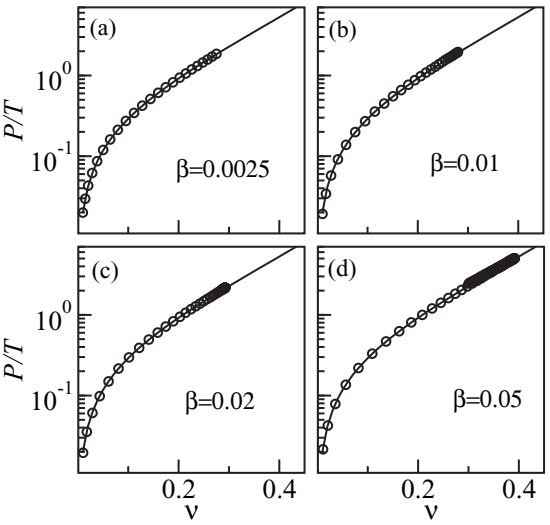

FIG. 16. Variation of P/T with ν for a constant-gravity system with a spatially varying temperature $T(x) = T_0\exp(-\beta x)$ with $T_0 = 20$ for different values of β indicated. The solid line denotes the predictions of the CS equation of state.

D. Analysis of Deviations between CS and MC Results

We consider here the deviations between the MC results and the predictions of the CS equation relative to the estimated numerical error of the MC simulations. We estimate the error in computing the pressure using MC simulations by carrying out N independent simulations to obtain N pressure profiles $[P_i(x)]$. The mean absolute error is then obtained as

$$\sigma(x) = \frac{1}{NP}\sum_{i=1}^{N}|P_i(x) - P(x)|, \tag{32}$$

where $P(x) = \sum_{i=1}^{N} P_i(x)/N$. The results reported are for $N = 5$, with each simulation result an average of 10^5 MCSs. We define the deviation (δ) as

$$\delta(x) = \frac{|P(x) - P_{CS}(x)|}{P_{CS}(x)}, \tag{33}$$

where $P_{CS}[\nu(x),T(x)]$ is the prediction of the CS equation.

Figure 17 shows the deviation (δ) and the error (σ) for the three different systems considered. For each system, only the case with the highest gradient is shown since the data are qualitatively similar for the remaining cases. The computational error in all cases is small ($\sigma < 2\times10^{-2}$, indicated by horizontal dotted lines in Fig. 17), except at low volume fractions where the number of particles is small.

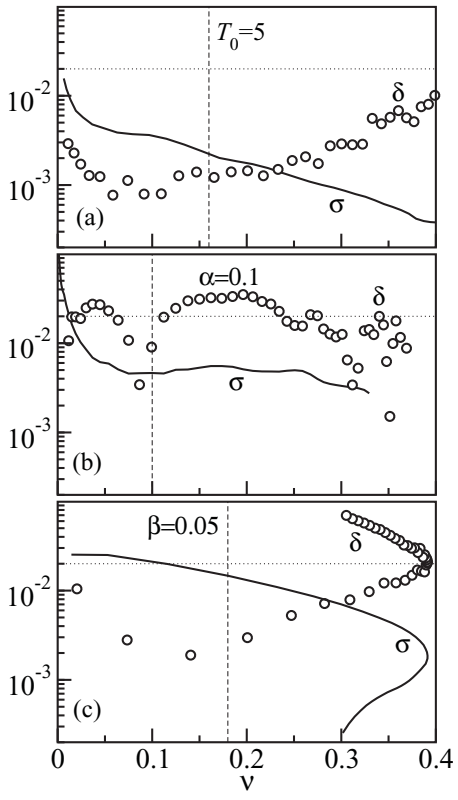

FIG. 17. Variation of δ and σ with ν for (a) an isothermal systems with constant gravity, (b) an isothermal system with a spatially varying gravitational field, and (c) a nonisothermal system with constant gravity for the parameter values indicated. The horizontal dotted lines correspond to a deviation of 2% and the vertical dashed lines to the value of volume fraction (ν) at which the gradient in number density (dn/dx) is highest.

The deviations between MC and CS (δ) are also small ($\delta \leqslant 2 \times 10^{-2}$) and are comparable to the reported accuracy of the CS equation ($\approx 10^{-2}$, [38]). The only exception to this is for $\beta = 0.05$ in the region of number density increasing with height ($x < x_m$, Fig. 14), where the deviation is as high as $\delta = 7 \times 10^{-2}$ (Fig. 17). Repeating the MC simulations with a bin of 0.05 particle diameters did not result in any change, and the reason for the larger-than-expected deviation is not clear. The deviations are of the same order as the computational error and are not higher in regions of high gradients (marked by vertical dashed lines in Fig. 17). The results presented here show the suitability of using gradient MC for high-throughput computations of thermodynamic properties.

V. SUMMARY AND DISCUSSION

Let us conclude this paper with a summary and discussion of the results presented here. We have presented a framework for gradient Monte Carlo (MC) simulations in systems with spatially varying temperature and external fields. Such simulations are relevant in a range of physical problems, including the flow of granular materials or powders. For the case with uniform temperature and a varying field, the usual MC prescription is appropriate. For the case with nonuniform temperature, we map this problem into one with uniform temperature and a space-dependent field. This method is generally applicable to fluids including the case of no applied field $g = 0$.

We use this framework to study a granular material consisting of hard spheres in a gravitational field. We consider cases with both uniform and nonuniform temperature. The gravity field settles the particles at the base of the system. The corresponding density profile [$n(x)$ vs x] is inhomogeneous with layering at the base — the precise profile is determined by the interplay between the external field and temperature. At low densities, the system shows ideal gas behavior. We also study the pressure-density profiles (P/T vs ν). Over a wide range of densities, the profiles obey the Carnahan-Starling (CS) equation of state. This validates the gradient MC method for the nonisothermal system. The deviations between MC and CS are found to be less than 2%, indicating the accuracy of the method in spite of significant number density gradients.

In general, the introduction of gradients in various parameters complicates a physical system. However, the presence of temperature and field gradients also enables us to access a wide range of pressure-density values (states) in a single simulation. This is reminiscent of high-throughput experimental methods, which study a multiplicity of states in a single experiment [39]. Gradient Monte Carlo is thus a useful approach for high-throughput computations of thermodynamic properties.

[1] K. Binder and D. W. Heerman, *Monte Carlo Simulation in Statistical Physics: An Introduction*, 4th ed. (Springer-Verlag, Berlin, 2002).

[2] M. E. J. Newman and G. T. Barkema, *Monte Carlo Methods in Statistical Physics* (Oxford University Press, Oxford, 1999).

[3] M. P. Allen and D. J. Tildesley, *Computer Simulation of Liquids* (Clarendon Press, Oxford, 1987).

[4] N. Metropolis and S. Ulam, J. Am. Stat. Assoc. **44**, 335 (1949).

[5] N. Metropolis, A. Rosenbluth, M. N. Rosenbluth, A. H. Teller, and E. Teller, J. Chem. Phys. **21**, 1087 (1953).

[6] G. A. Bird, *Molecular Gas Dynamics and the Direct Simulation of Gas Flows* (Clarendon, Oxford, 1994).

[7] H. M. Jaeger, S. R. Nagel, and R. P. Behringer, Rev. Mod. Phys. **68**, 1259 (1996).

[8] J. Duran, *Sands, Powders and Grains: An Introduction to the Physics of Granular Materials* (Springer Verlag, New York, 2000).

[9] G. H. Ristow, *Pattern Formation in Granular Materials* (Springer, Berlin, 2000).

[10] Y. Forterre and O. Pouliquen, Annu. Rev. Fluid Mech. **40**, 1 (2008).

[11] T. Biben, J.-P. Hansen, and J.-L. Barrat, J. Chem. Phys. **98**, 7330 (1993).

[12] T. Biben, R. Ohnesorge, and H. Lowen, Europhys. Lett. **28**, 665 (1994).

[13] M. Schmidt, M. Dijkstra, and J. P. Hansen, J. Phys. Condens. Matter **16**, S4185 (2004).

[14] V. A. Froltsov, C. N. Likos, H. Lowen, C. Eisenmann, U. Gasser, P. Keim, and G. Maret, Phys. Rev. E **71**, 031404 (2005).

[15] A. Mori, S. Yanagiya, Y. Suzuki, T. Sawada, and K. Ito, J. Chem. Phys. **124**, 174507 (2006).

[16] H. Chen and H. Ma, J. Chem. Phys. **125**, 024510 (2006).

[17] A. Cuetos, A. P. Hynninen, J. Zwanikken, R. van Roij, and M. Dijkstra, Phys. Rev. E **73**, 061402 (2006).

[18] M. Marechal and M. Dijkstra, Phys. Rev. E **75**, 061404 (2007).

[19] A. Torres, A. Cuetos, M. Dijkstra, and R. van Roij, Phys. Rev. E **75**, 041405 (2007).

[20] R. E. Beckham and M. A. Bevan, J. Chem. Phys. **127**, 164708 (2007).

[21] J. S. Vesaratchanon, A. Nikolov, D. Wasan, and D. Henderson, I&EC Res. **48**, 6641 (2009).

[22] T. Fricke and J. Schnakenberg, Zeitschrift fur Physik B Condensed Matter **83**, 277 (1991).

[23] P. Gengdi, X. Shijie, and C. Jianhua, Chin. Phys. Lett. **4**, 65 (1987).

[24] A. Rosato, K. J. Strandburg, F. Prinz, and R. H. Swendsen, Phys. Rev. Lett. **58**, 1038 (1987).

[25] H. J. Herrmann and M. Muller, Comput. Phys. Commun. **127**, 120 (2000).

[26] J. M. Ottino and D. V. Khakhar, Annu. Rev. Fluid Mech. **32**, 55 (2000).

[27] A. Coniglio, A. de Candia, A. Fierro, and M. Nicodemi, Physica A **344**, 431 (2004).

[28] C. K. K. Lun, S. Savage, D. J. Jeffrey, and N. Chepurniy, J. Fluid Mech. **140**, 223 (1984).

[29] J. T. Jenkins and F. Mancini, Phys. Fluids A **1**, 2050 (1989).

[30] D. V. Khakhar, J. J. McCarthy, and J. M. Ottino, Phys. Fluids **9**, 3600 (1997).

[31] D. V. Khakhar, J. J. McCarthy, and J. M. Ottino, Chaos **9**, 594 (1999).

[32] K. D. Seibert and M. A. Burns, AIChE J. **42**, 660 (1996).
[33] L. E. Silbert, D. Ertas, G. S. Grest, T. C. Halsey, D. Levine, and S. J. Plimpton, Phys. Rev. E **64**, 051302 (2001).
[34] J. Perrin, J. Phys. Theor. Appl. **9**, 5 (1910).
[35] N. V. Brilliantov and T. Poschel, *Kinetic Theory of Granular Gases* (Oxford University Press, Oxford, 2004).
[36] N. F. Carnahan and K. E. Starling, J. Chem. Phys. **51**, 635 (1969).
[37] R. Piazza, T. Bellini, and V. Degiorgio, Phys. Rev. Lett. **71**, 4267 (1993).
[38] M. Miandehy, H. Modarress, and M. R. Dehghani, Fluid Phase Equilibria **239**, 91 (2006).
[39] J. C. Meredith, A. Karim, and E. J. Amis, MRS Bull. **27**, 330 (2002).